Thermally induced spin-transfer torques in superconductor/ferromagnet bilayers

I. V. Bobkova,[1,2] A. M. Bobkov,[1] and Wolfgang Belzig[3]

[1] *Institute of Solid State Physics, Chernogolovka, Moscow reg., 142432 Russia*
[2] *Moscow Institute of Physics and Technology, Dolgoprudny, 141700 Russia*
[3] *Fachbereich Physik, Universität Konstanz, D-78457 Konstanz, Germany*

(Dated: September 11, 2019)

Thermally induced magnetization dynamics is currently a flourishing field of research due to its potential application in information technology. We study the paradigmatic system of a magnetic domain wall in a thermal gradient which is interacting with an adjacent superconductor. The spin-transfer torques arising in this system due to the combined action of the giant thermoelectric effect and the creation of equal-spin pairs in the superconductor are large enough to efficiently move the domain wall even in a ballistic situation. The mechanism is independent of hard to control impurity effects and paves the way to observe superconductivity-induced domain wall motion in realistic setups.

The essence of the thermoelectric or Seebeck effect is that a temperature gradient along a structure gives rise to a charge current and, hence, a bias voltage in an open circuit. However, in recent years a new paradigm has emerged by coupling spin and heat degrees of freedom – called spin caloritronics [1]. In particular, the spin Seebeck effect, that is the generation of a spin imbalance by a temperature gradient, has been discussed. Further, a thermally induced spin-transfer torque (STT), based on the spin-dependent Seebeck effect was predicted and its influence on the domain wall (DW) motion has been discussed[2–9]. The thermally induced STT can have at least two physical origins: (i) magnonic STT [10–12] and (ii) STT exerted by electronic quasiparticles [13, 14].

At low temperatures the main contribution to the thermally induced STT in ferromagnetic metals and semiconductors is the electronic one. The STT is generated by the thermally-induced electron spin flow. This spin flow can be quantified in terms of the spin thermopower $\nabla\mu_s/2e\nabla T$ generated by the temperature gradient ∇T in an open circuit, where $\mu_s = \mu_\uparrow - \mu_\downarrow$ is the spin imbalance of the spin-dependent chemical potentials. In order to have a nonzero spin current an electron-hole asymmetry at the Fermi level is required [1, 15–19]. Typically the corresponding electron-hole asymmetry in metallic ferromagnets is rather small resulting in the predicted spin thermopower $\mu_s/2e\nabla T = SP' \sim 10^{-3}$mV/K for intermetallic interfaces at room temperature [4, 20], while a much smaller spin thermopower $\sim 10^{-6}$mV/K was measured for a ferromagnetic film [19]. Here S is the thermopower and $P' = \partial_\varepsilon(G_\uparrow - G_\downarrow)|_{\varepsilon_F}/\partial_\varepsilon G|_{\varepsilon_F}$ is the polarization of the energy derivative of the conductance at the Fermi energy, $G_{\uparrow,\downarrow}$ is the spin-up (down) conductance and $G = G_\uparrow + G_\downarrow$. More recently, a very large thermopower and spin thermopower was predicted by lifting the spin degeneracy of the density of states in superconductors (e.g., by proximity to magnetic materials), [21–32]. The reason is that a huge spin-dependent particle-hole asymmetry in the superconductor is obtained in this case due to the presence of a superconducting gap. The observation of the large thermopower has been reported experimentally [33–35]. Upon application of strong in-plane magnetic fields $B \sim 1$T, Seebeck coefficients the order of 0.3mV/K were measured, what is comparable to the thermopower measured in magnetic semiconductors at much higher temperatures[36].

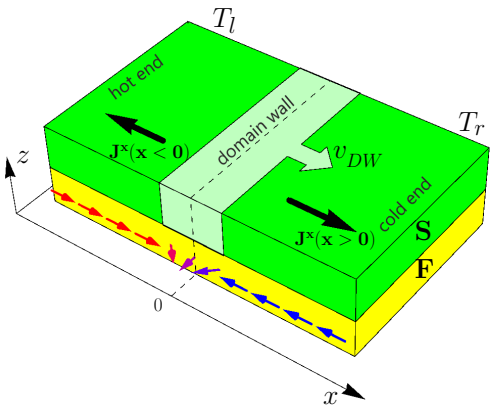

FIG. 1. Sketch of the bilayer S/F system. The magnetization of the F has a form of a head-to-head domain wall (DW) and is indicated by arrows. The picture on the top surface illustrates the process of thermally induced spin pumping into the DW region. Spin current in the bulk of the both domains is directed from the DW. In the right domain the directions of the spin current and the majority spin (opposite to the magnetization) flow coincide, while in the left domain they are opposite. Therefore, the majority spin always moves from the hot to the cold end. That means that the majority spin of the hotter domain is pumped into the DW region forcing the boundary between the domains to shift towards the cold end.

In spite of the impressive results on the Seebeck effect in S/F hybrids, the prospects of using the thermally induced spin currents to generate STT have not been explored so far. In the present Letter, we predict the existence of a thermally induced STT in thin film S/F bilayers containing a DW and investigate the resulting DW

motion. The origin of the STT is the electron spin flow in the superconductor due to a Zeeman splitting induced by the proximity of the ferromagnetic domains. Therefore, the STT is universal and is relevant for ferromagnetic metals as well as for magnetic insulators. Our results indicate that the role of superconducting elements in the STT is twofold. First, the giant spin Seebeck effect gives rise to an adiabatic torque component. However, the main finding is that the superconducting hybrids provide a unique mechanism for an anti-damping spin-transfer torque, which is not connected to spin-flip scattering of quasiparticles. The reason for the anti-damping STT is the presence of the superconducting condensate, which is sensitive to a gauge vector potential caused by a magnetic inhomogeneity and induces a spin current carried by equal-spin pairs. As a result of this pair-induced anti-damping STT the motion of an unpinned DW can be triggered by very small temperature gradients even in the ballistic case.

Model and method. The model system that we consider is shown in Fig. 1. It consists of a spin-textured ferromagnet with a spatially dependent magnetization $\boldsymbol{M}(\boldsymbol{r})$ in contact to a spin-singlet superconductor. The superconductor is assumed to be in the ballistic limit. The ferromagnet can be a metal or an insulator. If the thickness of the S film d_S is smaller than the superconducting coherence length ξ_S, the magnetic proximity effect, that is the influence of the adjacent ferromagnet on the S film can be described by adding the effective exchange field[37–42] $\boldsymbol{h}(\boldsymbol{r}) \sim -\boldsymbol{M}(\boldsymbol{r})$ to the quasiclassical Eilenberger equation, which we use below to treat the superconductor. While in general the magnetic proximity effect is not reduced to the effective exchange only [43–45], in the framework of the present study we neglect other terms which can be viewed as additional magnetic impurities in the superconductor and focus on the effect of the spin texture.

The bilayer film is assumed to be connected to equilibrium reservoirs having different temperatures $T_{l,r}$. We neglect all inelastic relaxation processes in the film assuming that its length is shorter than the corresponding relaxation length. As here we are dealing with a nonequilibrium problem, we work in the framework of the Keldysh technique for quasiclassical Green's functions. All the technical details of the Green's function calculation are given in the Supplementary Material. [46]

Below we are interested in the spin current flowing in the superconductor. It exerts a torque on the ferromagnet magnetization. The spin current of spin projection $\boldsymbol{J}$ in direction j can be calculated as follows:

$$\boldsymbol{J}_j = -\frac{N_F}{16}\int\limits_{-\infty}^{\infty} d\varepsilon \mathrm{Tr}_4\Big[\boldsymbol{\sigma}\langle v_{F,j}\check{g}^K\rangle\Big], \tag{1}$$

where $\check{g}^K(\epsilon, \boldsymbol{v}_F)$ represents the Keldysh part of the quasiclassical Green's function. N_F is the normal density of states at the Fermi level, $\langle\cdots\rangle$ implies averaging over the Fermi surface, and Tr_4 is the trace in Nambu⊗Spin space.

The torque can be calculated starting from the effective exchange interaction between the spin densities on the two sides of the S/F interface:

$$H_{int} = -\int d^2\boldsymbol{r} J_{ex}\boldsymbol{S}\boldsymbol{s}, \tag{2}$$

where $\boldsymbol{s}$ is the electronic spin density operator in the S film, $\boldsymbol{S}$ is the localized spin operator in the F film, J_{ex} is the exchange constant and the integration is performed over the 2D interface. It has been shown [45] that this exchange interaction Hamiltonian results in the appearance of the exchange field $h = J_{ex}M/(2\gamma d_s)$ in the S film. Here M is the saturation magnetization of the ferromagnet and γ is the gyromagnetic ratio.

Making use of the quantum kinetic equation for the electron Green's function in the S film, we find that for the case under consideration the spin density $\boldsymbol{s}$ obeys the following equation:

$$\partial_t \boldsymbol{s} = -\partial_j \boldsymbol{J}_j + 2\boldsymbol{h}\times\boldsymbol{s}, \tag{3}$$

where we have introduced the vector $\boldsymbol{J}_j = (J_j^x, J_j^y, J_j^z)$ corresponding to the spin current flowing along the j-axis in real space.

Applying Ehrenfest's theorem, one obtains the additional contribution to the Landau-Lifshitz-Gilbert equation from the exchange interaction Eq. (2) in the form of a torque acting on the magnetization:

$$\frac{\partial \boldsymbol{M}}{\partial t} = -\gamma\boldsymbol{M}\times\boldsymbol{H}_{\text{eff}} + \frac{\alpha}{M}\boldsymbol{M}\times\frac{\partial\boldsymbol{M}}{\partial t} + \frac{J_{ex}}{d_F}\boldsymbol{M}\times\boldsymbol{s}, \tag{4}$$

where α is the Gilbert damping constant and the last term represents the torque. $\boldsymbol{H}_{\text{eff}}$ is the local effective field

$$\boldsymbol{H}_{\text{eff}} = \frac{H_K M_x}{M}\boldsymbol{e}_x + \frac{2A}{M^2}\nabla^2\boldsymbol{M} - K_\perp M_z\boldsymbol{e}_z. \tag{5}$$

H_K is the anisotropy field, along the x-axis, A is the exchange constant and the self-demagnetization field $K_\perp M_z$ is included.

In a stationary situation $\partial_t\boldsymbol{s} = 0$ from Eq. (3) one can obtain that

$$\boldsymbol{N} = \frac{J_{ex}}{d_F}\boldsymbol{M}\times\boldsymbol{s} = \gamma\frac{d_S}{d_F}\partial_j\boldsymbol{J}_j. \tag{6}$$

To understand the efficiency of the torque $\boldsymbol{N}$ induced by the presence of the superconductor, we compare its value to the characteristic value of the torque induced by the effective field H_{eff}. Eq. (6) can be rewritten as $\boldsymbol{N}/\gamma H_K M = \zeta\partial_{\tilde{x}}\tilde{\boldsymbol{J}}_x$, with the dimensionless quantities $\partial_{\tilde{x}}\tilde{\boldsymbol{J}}_x = (2e^2R_N v_F/\Delta_0^2)\partial_x\boldsymbol{J}_x$ and $\zeta = E_S/\pi E_A$. The latter is proportional to the ratio of the condensation energy $E_S = N_F\Delta_0^2 d_S/2$ and the anisotropy energy $E_A = MH_K d_F/2$ per unit area of the film in the

(x, y)-plane. Here and below $R_N = \pi/(2e^2 N_F v_F)$ is the normal state resistance of the film and Δ_0 is the superconducting order parameter of the S film in the absence of the ferromagnet at zero temperature. Taking $E_S \sim d_S \times (10 \div 10^3)$ erg/cm^3 (for conventional superconductors like Al and Nb) and $E_A \sim d_F \times 10^5$ erg/cm^3 for Py thin films [47, 48] or $E_A \sim d_F \times (10 \div 10^2)$ erg/cm^3 for YIG thin films [49], we obtain that ζ can vary in a wide range $\zeta \sim (10^{-4} \div 10^2)(d_S/d_F)$.

Equilibrium spin current and superconductivity-induced DW deformation. The spin texture in the F can be parametrized as $\boldsymbol{M} = M(\cos\theta, \sin\theta\sin\delta, \sin\theta\cos\delta)$, where in general the both angles depend on x-coordinate. The equilibrium shape of the DW in the absence of the superconducting film is given by $\cos\theta = -\tanh(x/l_{\rm DW})$ and $\delta = \pi/2$, that is the DW is in (x, y)-plane.

It turns out that in the S/F bilayer with textured magnetization in the form of a plane DW a spontaneous spin current occurs in the region occupied by the wall. It is carried by the equal-spin Cooper pairs generated by the magnetic texture. The spin carried by this current is directed perpendicular to the DW plane, that is in our case in the z-direction (See details on the spontaneous spin current in the Supplementary material [46]). Similar spontaneous spin currents have already been obtained in the systems containing textured ferromagnets or homogeneous ferromagnets and spin-orbit coupling, presumably in the Josephson junction geometry [50–58]. The spin current is not conserved and exerts a torque on the magnetization. We find the resulting equilibrium shape of the DW from the LLG equation Eq. (4). It is found that the presence of the superconductor results in the appearance of the additional oscillations of the magnetization in the (x, y)-plane. These oscillations generate additional contributions to the in-plane effective field, which exerts a z-directed torque on the magnetization, thus compensating the action of the spontaneous spin current [46].

Thermally induced spin current in a homogeneous S/F bilayer. Now let us apply a temperature difference $T_l - T_r$ to the ends of the film. At first we consider a bilayer with a homogeneous magnetization without a DW. In this case a thermally induced spin current appears in the superconductor. This is a kind of a spin Seebeck effect. The spin current in the homogenous S/F bilayer only carries an x-spin component $J_x^x \equiv J$, which is directed along the ferromagnet magnetization. Fig. 2 demonstrates the dependence of the spin current on the cold (right) end temperature T_r at small $\delta T = T_l - T_r \ll T_r$ for different h. For a homogeneous bilayer the spin thermopower at $\delta T/\Delta_0 \ll 1$ can be readily found from Eq. (1)

$$\frac{2e^2 R_N J}{\delta T} = F\left(\frac{\Delta + h}{2T}\right) - F\left(\frac{\Delta - h}{2T}\right) \qquad (7)$$

with $F(x) = x\tanh x - \ln\cosh x$. The maximal values of $2eJR_N/\delta T$ are of the order of $(h/\Delta_0) \times 10^{-1}$mV/K

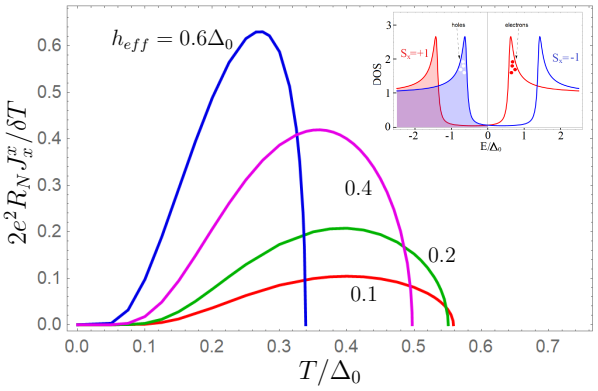

FIG. 2. Spin current divided by the temperature difference $\delta T \to 0$ in the homogeneous S/F bilayer vs the temperature. $h_{eff} = 0.1$(red), 0.2(green), 0.4(purple), 0.6(blue) in units of Δ_0. Insert: spin resolved DOS filled by thermally activated right-moving quasiparticles coming from the hot end. It is seen that all the right-moving quasiparticles contribute to spin flow of the same direction.

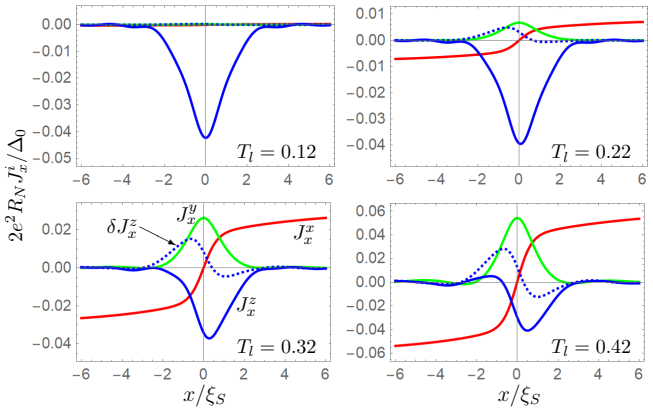

FIG. 3. Spatial profile of the spin current components J_x^x (red), J_x^y (green) and J_x^z (blue) for different temperatures of the hot end, $\delta J_x^z = J_x^z - J_x^z(T_l = T_r)$. $h_{eff} = 0.3\Delta_0$, $T_r = 0.02\Delta_0$, $l_{DW} = 0.5\xi_S$, where $\xi_S = v_F/\Delta_0$ throughout the paper.

and are reached for $T \sim 0.6 - 0.7T_c$, as illustrated in Fig. 2. The estimated values of $2eJR_N/\delta T$ are much larger than that ones obtained for nonsuperconducting systems containing metallic ferromagnets. Such large values of the spin Seebeck effect are a result of the huge spin-dependent electron-hole asymmetry close to the Fermi level, see the inset of Fig. 2. In fact, these estimates are close to the maximal possible value of the spin Seebeck effect, which can be reached if all the thermally induced quasiparticles (both electrons and holes) have the same spin. This optimal situation is realized in the present case of a Zeeman-split superconductor [23].

Thermally induced spin-transfer torque. The spatial profiles of the spin current for the plane DW (in the

(x, y)-plane) are presented in Fig. 3 for different temperatures of the hot end. At first, let us focus on J_x^x component, which is the only nonzero component of the thermally induced spin current in the bulk. Due to the presence of two magnetic domains with opposite magnetizations it leads to spin pumping into the region occupied by the DW. This process is schematically illustrated on the top surface of Fig. 1 and is described there.

We observe that the in-plane components J_x^x and J_x^y grow strongly when the temperature difference is increased. At the same time the temperature dependence of the out-of-plane J_x^z-component is much weaker. In the limit $T_l - T_r \to 0$ only J_x^z survives and the spin current coincides with the spontaneous spin current found in equilibrium.

The corresponding spatial profiles of the torque components can be easily deduced as spatial derivatives of the corresponding spin current components $\boldsymbol{N}_i = \gamma(d_S/d_F)\partial_x J_x^i$. For a nonsuperconducting ferromagnetic system the thermally induced spin torque can be written as [5] $\boldsymbol{N} = a\ \partial_x \boldsymbol{m} + b\ \boldsymbol{m} \times \partial_x \boldsymbol{m}$, where $\boldsymbol{m} = \boldsymbol{M}/M$. Both coefficients a and b are phenomenological parameters. They are proportional to the temperature gradient in the framework of the linear response theory. The first (second) term can be related to electron spins following (mistracking) the magnetic texture. Therefore, a accounts for the adiabatic contribution to the torque and b describes the nonadiabatic contribution.

For the S/F bilayer the adiabatic contribution to the torque results from the spin pumping process described above. The non-adiabatic contribution, which for the plane DW is $N_z \sim \partial_x J_x^z$, is nonzero even for the ballistic case. It indicates that the physical nature of this contribution is strongly different from that in nonsuperconducting systems. While in nonsuperconducting systems the origin of the nonadiabatic torque is connected to spin-flip processes, here we don't have any spin-flip processes and the nonadiabatic contribution is generated by a spin current carried by spin-triplet pars in the region of the DW. This is also seen by the fact that the nonadiabatic torque does not vanish at $\delta T \to 0$ contrary to the nonsuperconducting situation. In equilibrium it is compensated by the additional contributions to the in-plane effective field due to the DW shape distortion, as we described above. However, any deviation of the DW shape from the equilibrium shape immediately results in the appearance of an uncompensated nonadiabatic torque.

Thermally induced DW motion. The dynamics of the DW under the applied temperature difference is calculated from the LLG Eq. (4). At the present study we focus on small values of the parameter ζ describing how strong is the torque induced by the superconductor. In this case we calculate the torque for the unperturbed DW neglecting the distortion of the DW shape due to the presence of the superconductor. Our numerical results for the spatial profiles of the moving DW demonstrate that the distortion is indeed very small, therefore justifying the above assumption.

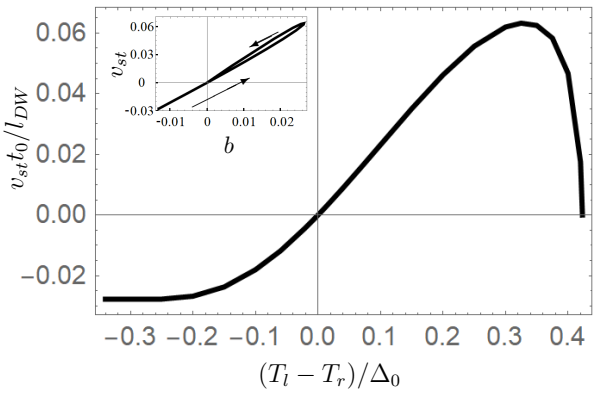

FIG. 4. DW velocity v_{st} as a function of $\delta T = T_l - T_r$. $t_0 = (\gamma H_K)^{-1}$. Insert: v_{st} as a function of $b(x = x_{DW})$. The direction of δT growing along this curve is marked by the arrow. $\zeta = 0.3$, $\alpha = 0.2$, $K_\perp = H_K/M$, $T_r = 0.35\Delta_0$.

We found that for the values of ζ and $T_l - T_r$ considered in Fig. 4 the DW moves as a rigid object reaching the steady state at a characteristic time $t_d = 1/4\pi\alpha\gamma M$. For the considered parameters we have found no sign of a precessional motion. The steady state velocity v_{st} as a function of δT is plotted in Fig. 4. We see that at $\delta T \ll \Delta_0$ the velocity is a linear function of the temperature difference. For nonsuperconducting systems it is well-known that the stationary DW motion at small applied currents or temperature gradients is provided by the non-adiabatic torque contribution[59]. Here the situation is very similar. An essential feature of the superconducting system is that the microscopically calculated coefficients a and b are spatially dependent, see supplementary material [46] for details. Nevertheless, $v_{st} \sim b(x = x_{DW}) = -l_{DW} N_z(x = x_{DW})$, as it is demonstrated in the insert to Fig. 4 (x_{DW} is the DW center position at a given time). The hysteretic behavior of the line is due to the nonmonotonic dependence of the velocity, as well as $b(x_{DW})$ on δT, which in turn results from the suppression of superconductivity by heating of the film.

The DW velocity v_{st} is linearly proportional to the S/F coupling strength ζ. At $\zeta = 0.3$ and taking material parameters for Py films[48] $H_K = 500$Oe and $l_{DW} = 20$nm or for YIG thin films[49] $H_K \sim 0.5$Oe and $l_{DW} = 1\mu$m the maximal DW velocities can be estimated from Fig. 4 as $v_{Py} \sim 200$m/s and $v_{YIG} \sim 10$m/s. In these estimates we take into account that $v_{st} \sim \alpha^{-1}$ and realistic values of $\alpha \sim 0.01$.

In summary, we have predicted and microscopically calculated a thermally induced STT in thin film S/F bilayers containing a DW. It features adiabatic as well nonadiabatic contributions. The former results from the thermally induced spin pumping into the superconduct-

ing region close to the DW. The physical mechanism of the latter is a unique feature of superconducting hybrids: it is caused by the presence of a spatially dependent spin current carried by triplet Cooper pairs in the region occupied by the DW. We have demonstrated that this torque contribution allows for the steady DW motion at small temperature differences.

Acknowledgments. This work was financially supported by the DFG through SFB 767 *Controlled Nanosystems*. The work of A.M.B and I.V.B is carried out within the state task of ISSP RAS. I.V.B. also acknowledges the financial support by Foundation for the Advancement of Theoretical Physics and Mathematics BASIS.

SUPPLEMENTARY MATERIAL

Quasiclassical Keldysh Green's functions technique in terms of Riccati parametrization

The matrix Green's function $\check{g}(\boldsymbol{r},\boldsymbol{p}_F,\varepsilon,t)$ is a 8×8 matrix in the direct product of spin, particle-hole and Keldysh spaces and depends on the spatial vector $\boldsymbol{r}$, quasiparticle momentum direction $\boldsymbol{p}_F$, quasiparticle energy ε and time t. In the S film it obeys the Eilenberger equation:

$$i\boldsymbol{v}_F\nabla\check{g}(\boldsymbol{r},\boldsymbol{p}_F)+\left[\varepsilon\tau_z+\boldsymbol{h}(\boldsymbol{r})\boldsymbol{\sigma}\tau_z-\check{\Delta},\check{g}\right]_{\otimes}=0, \qquad (8)$$

where $[A,B]_{\otimes}=A\otimes B-B\otimes A$ and $A\otimes B=\exp[(i/2)(\partial_{\varepsilon_1}\partial_{t_2}-\partial_{\varepsilon_2}\partial_{t_1})]A(\varepsilon_1,t_1)B(\varepsilon_2,t_2)|_{\varepsilon_1=\varepsilon_2=\varepsilon;t_1=t_2=t}$. $\tau_{x,y,z}$ are Pauli matrices in particle-hole space with $\tau_{\pm}=(\tau_x\pm i\tau_y)/2$. $\hat{\Delta}=\Delta(x)\tau_+-\Delta^*(x)\tau_-$ is the matrix structure of the superconducting order parameter $\Delta(x)$ in the particle-hole space.

In the ballistic case, it is convenient to use the so-called Riccati parametrization for the Green's function [60, 61]. In terms of the Riccati parametrization the retarded Green's function takes the form:

$$\check{g}^{R,A}=\pm N^{R,A}\otimes\begin{pmatrix}1-\hat{\gamma}^{R,A}\otimes\hat{\tilde{\gamma}}^{R,A} & 2\hat{\gamma}^{R,A}\\ 2\hat{\tilde{\gamma}}^{R,A} & -(1-\hat{\tilde{\gamma}}^{R,A}\otimes\hat{\gamma}^{R,A})\end{pmatrix}, \qquad (9)$$

$$\check{g}^{K}=2N^{R}\otimes\begin{pmatrix}x^K+\hat{\gamma}^R\otimes\hat{\tilde{x}}^K\otimes\hat{\tilde{\gamma}}^A & -(\hat{\gamma}^R\otimes\hat{\tilde{x}}^K-\hat{x}^K\hat{\gamma}^A)\\ \hat{\tilde{\gamma}}^R\otimes\hat{x}^K-\hat{\tilde{x}}^K\otimes\hat{\tilde{\gamma}}^A & \hat{\tilde{x}}^K+\hat{\tilde{\gamma}}^R\otimes\hat{x}^K\otimes\hat{\gamma}^A)\end{pmatrix}\otimes N^A \qquad (10)$$

with

$$N^{R,A}=\begin{pmatrix}1+\hat{\gamma}^{R,A}\otimes\hat{\tilde{\gamma}}^{R,A} & 0\\ 0 & 1+\hat{\tilde{\gamma}}^{R,A}\otimes\hat{\gamma}^{R,A}\end{pmatrix}^{-1} \qquad (11)$$

where $\hat{\gamma}^{R,A}$, $\hat{\tilde{\gamma}}^{R,A}$, $\hat{x}^K$ and $\hat{\tilde{x}}^K$ are matrices in spin space. Note that our parametrization differs from the definition in the literature [60, 61] by factors $i\sigma_y$ as $\hat{\gamma}^{R,A}_{standard}=\hat{\gamma}^{R,A}i\sigma_y$ and $\hat{\tilde{\gamma}}^{R,A}_{standard}=i\sigma_y\hat{\tilde{\gamma}}^{R,A}$. The Riccati parametrization Eq. (9) obeys the normalization condition $\check{g}\otimes\check{g}=1$ automatically.

The Riccati amplitude $\hat{\gamma}$ obeys the following Riccati-type equations:

$$i\boldsymbol{v}_F\nabla\hat{\gamma}^R+2\varepsilon\hat{\gamma}^R=-\hat{\gamma}^R\otimes\Delta^*\otimes\hat{\gamma}^R-\left\{\boldsymbol{h}\boldsymbol{\sigma},\hat{\gamma}^R\right\}_{\otimes}-\Delta \qquad (12)$$

and $\hat{\tilde{\gamma}}$ obeys the same equation with the substitution $\varepsilon\to-\varepsilon$, $\boldsymbol{h}\to-\boldsymbol{h}$ and $\Delta\to\Delta^*$.

The distribution function $\hat{x}^K$ obeys the equation:

$$i\boldsymbol{v}_F\nabla\hat{x}^K+i\partial_t\hat{x}^K+\hat{\gamma}^R\otimes\Delta^*\otimes\hat{x}^K+\hat{x}^K\otimes\Delta\otimes\hat{\tilde{\gamma}}^A+[\boldsymbol{h}\boldsymbol{\sigma},\hat{x}^K]_{\otimes}=0, \qquad (13)$$

while $\hat{\tilde{x}}^K$ obeys the same equation with the substitution $\boldsymbol{h}\to-\boldsymbol{h}$, $\Delta\to\Delta^*$, $\hat{\gamma}^{R,A}\leftrightarrow\hat{\tilde{\gamma}}^{R,A}$. In this work, we assume $\Delta=\Delta^*$.

If we consider a locally spatially inhomogeneous magnetic texture like a domain wall, the Riccati amplitudes $\hat{\gamma}$ and $\hat{\tilde{\gamma}}$ can be found from Eq. (12) numerically with the following asymptotic condition:

$$\hat{\gamma}_\infty=\gamma_{0\infty}+\frac{\boldsymbol{h}_\infty\boldsymbol{\sigma}}{h}\gamma_\infty, \qquad (14)$$

$$\gamma_{0\infty}=-\frac{1}{2}\Big[\frac{\Delta}{\varepsilon+h+i\sqrt{\Delta^2-(\varepsilon+h)^2}}+\frac{\Delta}{\varepsilon-h+i\sqrt{\Delta^2-(\varepsilon-h)^2}}\Big], \qquad (15)$$

$$\gamma_\infty=-\frac{1}{2}\Big[\frac{\Delta}{\varepsilon+h+i\sqrt{\Delta^2-(\varepsilon+h)^2}}-\frac{\Delta}{\varepsilon-h+i\sqrt{\Delta^2-(\varepsilon-h)^2}}\Big], \qquad (16)$$

and $\hat{\tilde{\gamma}}_\infty=-\hat{\gamma}_\infty$.

Eq. (12) is numerically stable if it is solved starting from $x=-\infty$ for right-going trajectories $v_x>0$ and from $x=+\infty$ for left-going trajectories $v_x<0$. On the contrary, $\hat{\tilde{\gamma}}$ can be found numerically starting from $x=+\infty$ for right-going trajectories $v_x>0$ and from $x=-\infty$ for left-going trajectories $v_x<0$. The advanced Riccati amplitudes can be found taking into account the relation [61] $\hat{\gamma}^A=-(\hat{\tilde{\gamma}}^R)^\dagger$. The superconducting order parameter is to be found self-consistently according to

$$\Delta=-\frac{\lambda}{8}\int\limits_{-\Omega}^{\Omega}d\varepsilon\mathrm{Tr}_4\langle\tau_-\check{g}^K\rangle, \qquad (17)$$

where $\langle...\rangle$ means averaging over the Fermi surface, λ is the coupling constant and Ω is the Debye frequency cutoff.

If we neglect the dependence of $\boldsymbol{h}$ on time, then it follows from Eq. (13) that the distribution function $\hat{x}^K$ for

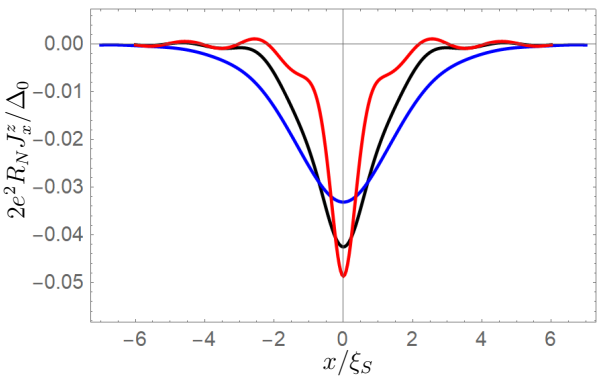

FIG. 5. Spin current $J_x^z(x)$ at the plane DW in equilibrium. Other components of the spin current are zero. $l_{DW} = \xi_S$(blue); $0.5\xi_S$(black); $0.2\xi_S$(red). $\xi_S = v_F/\Delta_0$ throughout the paper. $h_{eff} = 0.3\Delta_0$, $T = 0.02\Delta_0$.

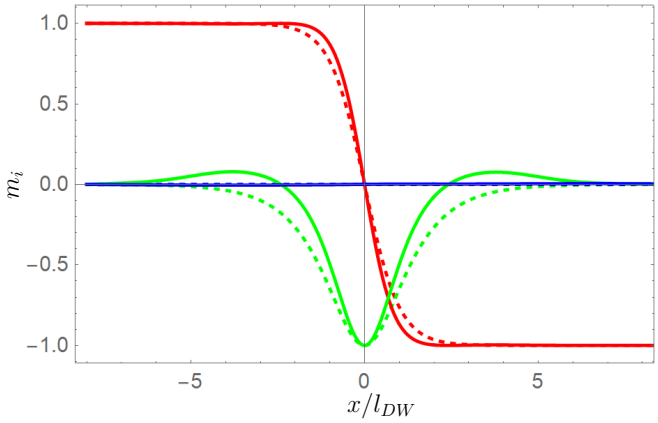

FIG. 6. Magnetization profile in the equilibrium S/F bilayer for $\zeta = 10$. $\boldsymbol{m}_i = \boldsymbol{M}_i/M$. Different magnetization components are plotted in different colors: m_x-red, m_y-green and m_z-blue. The dotted curves correspond to $\zeta = 0$ (the superconductor is absent). $l_{DW} = 0.5\xi_S$, $h_{eff} = 0.3\Delta_0$, $T = 0.02\Delta_0$, $K_\perp = H_K/M$.

a given ballistic trajectory is determined by the equilibrium distribution function of the left (right) reservoir for $v_{F,x} > 0$ ($v_{F,x} < 0$) and takes the form

$$\hat{x}_\pm^K = (1 + \hat{\gamma}_\pm^R \otimes \hat{\tilde{\gamma}}_\pm^A) \tanh \frac{\varepsilon}{2T_{l,r}}, \tag{18}$$

where the subscript $+(-)$ corresponds to the trajectories $v_{F,x} > 0$ ($v_{F,x} < 0$). On the contrary,

$$\hat{\tilde{x}}_\pm^K = -(1 + \hat{\tilde{\gamma}}_\pm^R \otimes \hat{\gamma}_\pm^A) \tanh \frac{\varepsilon}{2T_{r,l}}. \tag{19}$$

The terms $\propto \dot{\boldsymbol{h}}$ in Eq. (13) can be neglected under the condition $(h/\Delta)(1/t_d\Delta) \ll 1$, where t_d is the characteristic time of the induced magnetization dynamics. For realistic parameters $t_d \sim 10^{-9} - 10^{-8}c$. Therefore, at $\Delta \sim 1K$ and $h/\Delta \lesssim 1$ this condition is fulfilled to a good accuracy. Physically, these terms account for the electromotive force, which arises in the system due to the magnetization dynamics and has been studied in different contexts before [62–74], but here its back influence on the magnetization dynamics can be safely neglected.

Spontaneous spin current, DW magnetization profile and self-consistent superconducting order parameter in equilibrium S/F bilayer

The spontaneous spin current for our ballistic S film in proximity to the ferromagnet with a coplanar DW is plotted in Fig. 5. It is seen that the amplitude of the spontaneous current is higher for narrow DWs. In the limit $l_{DW}/\xi_S \gg 1$ it disappears. The spin current is not conserved and exerts a spin-transfer torque on the magnetization. We find the resulting equilibrium shape of the DW accounting for the spin-transfer torque from the LLG equation. It is found that the presence of the superconductor results in the appearance of the additional oscillations of the magnetization in the (x, y)-plane. These oscillations generate additional contributions to the in-plane effective field, which exerts a z-directed torque on the magnetization, thus compensating the action of the spontaneous spin current. The resulting magnetization profile in equilibrium is presented in Fig. 6. For realistic ratios of the anisotropy field to the demagnetization field $H_K/K_\perp M$ we have found no noticeable deviation of the DW shape from the initial (x, y)-plane. At the same time the distortion of the DW is accompanied by its narrowing, which also appears to provide appropriate contributions to the in-plane effective field. It is worth noting that Fig. 6 is plotted for the extremely high value of $\zeta = 10$ to make the distortions clearly visible.

Equilibrium S/F bilayer with a DW was previously considered for a dirty system in Ref. 58 based on the free energy consideration. For a trial Neel-type plane DW it was found that the presence of the superconductor shrinks the DW size. This effect is closely connected to the fact that the the superconductivity can be enhanced for narrow DWs due to the effective averaging of the exchange field, and, consequently, to weaker suppression of superconductivity in the DW region. The increase of the superconducting order parameter provides the corresponding gain in the condensation energy. Here we do not see this effect because the considered exchange fields and temperatures are too small to cause essential suppression of the order parameter far from the DW, what is a necessary condition to have the superconductivity enhancement (restoring) near the DW. Instead, we observe weak Friedel-like oscillations of the order parameter near the DW and suggest that it is a specific feature of the ballistic limit we consider.

The self-consistent profile of the order parameter calculated in the presence of a DW in the F layer is demon-

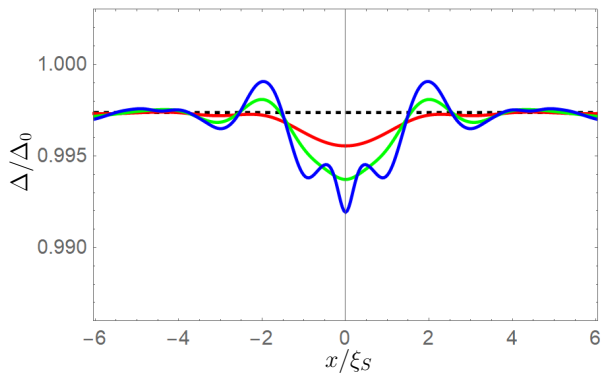

FIG. 7. Self-consistent order parameter as a function of the spatial coordinate along the bilayer. $l_{DW} = \xi_S$(red); $0.5\xi_S$(green); $0.2\xi_S$(blue). $h_{eff} = 0.3\Delta_0$. Black dotted line represents the order parameter value in the S/F bilayer in the absence of a DW.

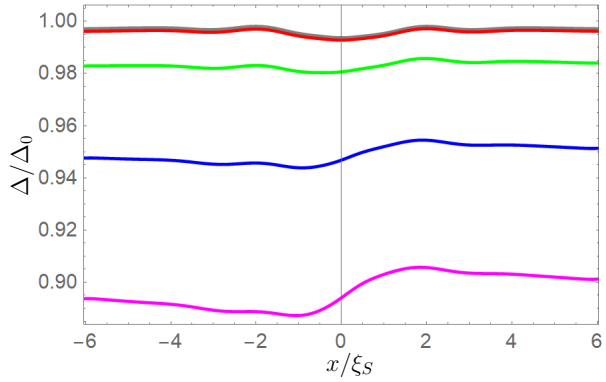

FIG. 8. Self-consistent profile of the order parameter in the presence of the DW and a temperature difference. Different curves correspond to different temperatures of the hot end $T_l = 0.02\Delta_0$(grey), 0.12(red), 0.22(green), 0.32(blue) and 0.42(purple). $h_{eff} = 0.3\ \Delta_0$, $T_r = 0.02\Delta_0$, $l_{DW} = 0.5\xi_S$.

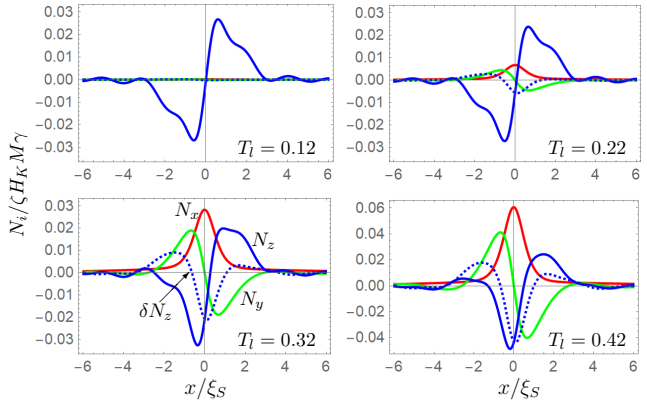

FIG. 9. Spatial profile of the torque components N_x (red), N_y (green) and N_z (blue) at the plane DW under the applied heat bias, $\delta N_z = N_z - N_z(T_l = T_r)$. $h_{eff} = 0.3\Delta_0$, $T_r = 0.02\Delta_0$, $l_{DW} = 0.5\xi_S$.

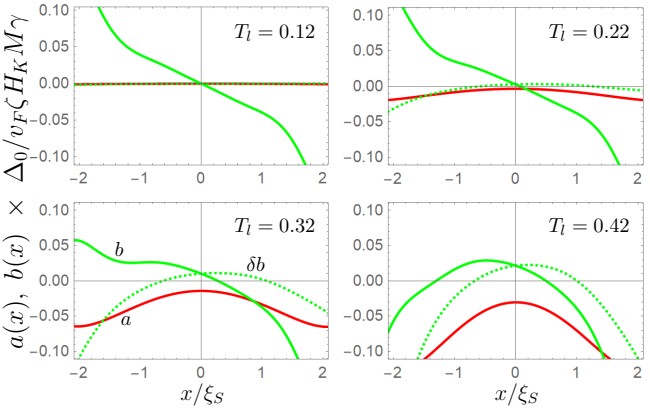

FIG. 10. Torque coefficients $a(x)$(red) and $b(x)$(green) for different temperatures of the hot end, $\delta b = b - b(T_l = T_r)$. $h_{eff} = 0.3\Delta_0$, $T_r = 0.02\Delta_0$, $l_{\rm DW} = 0.5\xi_S$.

strated in Fig. 7 for three different DW widths. It is seen that it manifests Friedel-like oscillating behavior. The oscillations become more pronounced for narrow DWs, but are generally weak for considered values of the suppression factors: exchange field and temperature.

Details of the order parameter and torque calculations under the applied temperature difference

At first in Fig. 8 we demonstrate results for the self-consistent profile of the superconducting order parameter in the presence of the DW and a temperature difference. The small overall suppression of the order parameter by heating of the superconductor is clearly seen. More interesting feature is that the order parameter is additionally suppressed near the DW from the "hotter" side and slightly enhanced with respect to the bulk value from the "colder" side of the DW. It seems that there appears an excess (lack) of quasiparticles at the corresponding side of the DW.

The spatial profiles of the torque $\boldsymbol{N}$ acting on the DW from the spatially-dependent spin current, shown in Fig. 3 of the main text, are presented in Fig. 9. In order to investigate the structure of the torque induced by the presence of the superconductor, we separate it to adiabatic $a\partial_x\boldsymbol{m}$ and nonadiabatic $b\boldsymbol{m}\times\partial_x\boldsymbol{m}$ contributions. In fact, the full microscopic result obtained from Eq. (6) of the main text also contains the term $\sim \boldsymbol{m}$, but we exclude this contribution because in the framework of the considered model the amplitude of the magnetization is fixed.

The essential feature of the superconducting system is that the microscopically calculated coefficients a and b in our case are spatially dependent. They are plotted in

Fig. 10 as functions of x-coordinate (the DW center is at $x = 0$) for different temperatures of the hot end. It is different from the nonsuperconducting case, where they are typically do not depend on coordinates due to absence of a corresponding spatial scale. Here the characteristic scale of the spatial variation of a and b is determined by the superconducting coherence length ξ_S. It is interesting that the coefficient b is even a sign-changing function of the x-coordinate. In equilibrium, at $T_l = T_r$, $b = 0$ at $x = x_{DW}$, that is, in the center of the DW. Under the applied temperature difference it is useful to introduce $\delta b = b - b(T_l = T_r)$. It becomes nonzero at $x = x_{DW}$: $\delta b(x = x_{DW}) = b(x = x_{DW}) \neq 0$. The DW velocity is proportional to this quantity as it is demonstrated in the main text.

[1] G. Bauer, E. Saitoh, and B.J. van Wees, Spin caloritronics, Nat. Mat. **11**, 391 (2012).

[2] L. Berger, Thermal forces on ferromagnetic domain walls, associated with the wall entropy, J. Appl. Phys. **58**, 450 (1985).

[3] S. U. Jen and L. Berger, Thermal domain drag effect in amorphous ferromagnetic materials. I. Theory, J. Appl. Phys. **59**, 1278 (1986).

[4] M. Hatami, G. E.W. Bauer, Q. Zhang and P. J. Kelly, Thermal Spin-Transfer Torque in Magnetoelectronic Devices, Phys. Rev. Lett. **99**, 066603 (2007).

[5] A. A. Kovalev and Y. Tserkovnyak, Thermoelectric spin transfer in textured magnets, Phys. Rev. B **80**, 100408 (2009).

[6] D. Hinzke and U. Nowak, Domain Wall Motion by the Magnonic Spin Seebeck Effect, Phys. Rev. Lett. **107**, 027205 (2011).

[7] P. Yan, X. S. Wang, and X. R. Wang, All-Magnonic Spin-Transfer Torque and Domain Wall Propagation, Phys. Rev. Lett. **107**, 177207 (2011).

[8] K. M.D. Hals, A. Brataas, and G. E.W. Bauer, Thermopower and thermally induced domain wall motion in (Ga, Mn)As, Solid State Comm. **150**, 461 (2010).

[9] S. Moretti, V. Raposo, E. Martinez, and L.s Lopez-Diaz, Domain wall motion by localized temperature gradients, Phys. Rev. B **95**, 064419 (2017).

[10] J. Torrejon, G. Malinowski, M. Pelloux, R. Weil, A. Thiaville, J. Curiale, D. Lacour, F. Montaigne, and M. Hehn, Unidirectional Thermal Effects in Current-Induced Domain Wall Motion, Phys. Rev. Lett. **109**, 106601 (2012).

[11] W. Jiang, P. Upadhyaya, Y. Fan, J. Zhao, M. Wang, Li-Te Chang, M. Lang, K. L. Wong, M. Lewis, Y.-T. Lin, J. Tang, S. Cherepov, X. Zhou, Y. Tserkovnyak, R. N. Schwartz, and K. L. Wang, Direct Imaging of Thermally Driven Domain Wall Motion in Magnetic Insulators, Phys. Rev. Lett. **110**, 177202 (2013).

[12] A. J. Ramsay, P. E. Roy, J. A. Haigh, R. M. Otxoa, A. C. Irvine, T. Janda, R. P. Campion, B. L. Gallagher, and J. Wunderlich, Optical Spin-Transfer-Torque-Driven Domain-Wall Motion in a Ferromagnetic Semiconductor, Phys. Rev. Lett. **114**, 067202 (2015).

[13] H. Yu, S. Granville, D. P. Yu, and J.-Ph. Ansermet, Evidence for Thermal Spin-Transfer Torque, Phys. Rev. Lett. **104**, 146601 (2010).

[14] A. Pushp, T. Phung, C. Rettner, B. P. Hughes, See-Hun Yang, and S. S. P. Parkin, Giant thermal spin-torqueassisted magnetic tunnel junction switching, PNAS **112**, 6585 (2015).

[15] M. Johnson and R. H. Silsbee, Thermodynamic analysis of interfacial transport and of the thermomagnetoelectric system, Phys. Rev. B **35**, 4959 (1987); M. Johnson, ChargeSpin Coupling at a FerromagnetNonmagnet Interface, J. Supercond. **16**, 679 (2003).

[16] L. Gravier, S. Serrano-Guisan, F. Reuse, and J.-P. Ansermet, Thermodynamic description of heat and spin transport in magnetic nanostructures, Phys. Rev. B **73**, 024419 (2006); Spin-dependent Peltier effect of perpendicular currents in multilayered nanowires, Phys. Rev. B **73**, 052410 (2006).

[17] K. Uchida, J. Xiao, H. Adachi, J. Ohe, S. Takahashi, J. Ieda, T. Ota, Y. Kajiwara, H. Umezawa, H. Kawai, G. E. W. Bauer, S. Maekawa, and E. Saitoh, Spin Seebeck insulator, Nature Mater., **9**, 894 (2010).

[18] 37 A. Slachter, F. Bakker, J. Adam, and B.J. van Wees, Thermally driven spin injection from a ferromagnet into a non-magnetic metal, Nature Phys. **6**, 879 (2010).

[19] K. Uchida, S. Takahashi, K. Harii, W. Koshibae, K. Ando, S. Maekawa and E. Saitoh, Observation of the spin Seebeck effect, Nature, **455**, 778 (2008).

[20] M. Hatami, G. E.W. Bauer, Q. Zhang and P. J. Kelly, Thermoelectric effects in magnetic nanostructures, Phys. Rev. B **79**, 174426 (2009).

[21] P. Machon, M. Eschrig, and W. Belzig, Nonlocal Thermoelectric Effects and Nonlocal Onsager relations in a Three-Terminal Proximity-Coupled Superconductor-Ferromagnet Device, Phys. Rev. Lett. **110**, 047002 (2013).

[22] M. S. Kalenkov, A. D. Zaikin, and L. S. Kuzmin, Theory of a Large Thermoelectric Effect in Superconductors Doped with Magnetic Impurities, Phys. Rev. Lett. **109**, 147004 (2012).

[23] A. Ozaeta, P. Virtanen, F.S. Bergeret, and T.T. Heikkila, Predicted Very Large Thermoelectric Effect in Ferromagnet-Superconductor Junctions in the Presence of a Spin-Splitting Magnetic Field, Phys. Rev. Lett. **112**, 057001 (2014).

[24] F. Giazotto, J. W. A. Robinson, J. S. Moodera, and F. S. Bergeret, Proposal for a phase-coherent thermoelectric transistor, Appl. Phys. Lett. **105**, 062602 (2014).

[25] M. S. Kalenkov and A. D. Zaikin, Enhancement of thermoelectric effect in diffusive superconducting bilayers with magnetic interfaces, Phys. Rev. B **91**, 064504 (2015).

[26] P. Machon, M. Eschrig, and Belzig, Giant thermoelectric effects in a proximity-coupled superconductorferromagnet device, New J. Phys. **16**, 073002 (2014).

[27] S. Kawabata, A. Ozaeta, A. S. Vasenko, F. W. J. Hekking, and F. S. Bergeret, Efficient electron refrigeration using superconductor/spin-filter devices, Appl. Phys. Lett. **103**, 032602 (2013).

[28] F. Giazotto, T. T. Heikkila, and F. S. Bergeret, Very Large Thermophase in Ferromagnetic Josephson Junctions, Phys. Rev. Lett. **114**, 067001 (2015).

[29] J. Linder, M.E. Bathen, Spin caloritronics with superconductors: Enhanced thermoelectric effects, generalized Onsager response-matrix, and thermal spin currents,

Phys. Rev. B **93**, 224509 (2016).
[30] I. V. Bobkova and A. M. Bobkov, Thermospin effects in superconducting heterostructures, Phys. Rev. B **96**, 104515 (2017).
[31] A Rezaei, A. Kamra, P. Machon, and W. Belzig, Spin-flip enhanced thermoelectricity in superconductor-ferromagnet bilayers, New J. Phys. **20**, 073034 (2018).
[32] F. Aikebaier, M. A. Silaev, T. T. Heikkila, Supercurrent-induced charge-spin conversion in spin-split superconductors, Phys. Rev. B **98**, 024516 (2018).
[33] S. Kolenda, M. J. Wolf, and D. Beckmann, Observation of Thermoelectric Currents in High-Field Superconductor-Ferromagnet Tunnel Junctions, Phys. Rev. Lett. **116**, 097001 (2016).
[34] S. Kolenda, C. Surgers, G. Fischer, and D. Beckmann, Thermoelectric effects in superconductor-ferromagnet tunnel junctions on europium sulfide, Phys. Rev. B **95** 224505 (2017).
[35] S. Kolenda, P. Machon, D. Beckmann, and W. Belzig, Nonlinear thermoelectric effects in high-field superconductor-ferromagnet tunnel junctions, Beilstein J. Nanotechnol. **7** 1579 (2016).
[36] Y. Pu, D. Chiba, F. Matsukura, H. Ohno, J Shi, Mott Relation for Anomalous Hall and Nernst Effects in $Ga_{1-x}Mn_xAs$ Ferromagnetic Semiconductors, Phys. Rev. Lett. **101** 117208 (2008).
[37] L. N. Bulaevskii, A. I. Buzdin, and S. V. Panjukov, The oscillation dependence of the critical current on the exchange field of ferromagnetic metals (F) in Josephson junction S-F-S, Solid State Commun. **44**, 539 (1982).
[38] W. Belzig, A. Brataas, Y. Nazarov, and G. Bauer, Spin accumulation and Andreev reflection in a mesoscopic ferromagnetic wire, Phys. Rev. B **62**, 9726 (2000).
[39] F.S. Bergeret, A.F. Volkov, and K.B. Efetov, Odd triplet superconductivity and related phenomena in superconductor-ferromagnet structures, Rev. Mod. Phys. **4**, 1321 (2005).
[40] A. I. Buzdin, Proximity effects in superconductor-ferromagnet heterostructures, Rev. Mod. Phys. **77**, 935 (2005).
[41] T. Tokuyasu, J. A. Sauls, and D. Rainer, Proximity effect of a ferromagnetic insulator in contact with a superconductor, Phys. Rev. B **38**, 8823 (1988).
[42] A. Millis, D. Rainer, and J. A. Sauls, Quasiclassical theory of superconductivity near magnetically active interfaces, Phys. Rev. B **38**, 4504 (1988).
[43] A. Cottet, D. Huertas-Hernando, W. Belzig, and Yu.V. Nazarov, Spin-dependent boundary conditions for isotropic superconducting Greens functions, Phys. Rev. B **80**, 184511 (2009) [Erratum: Phys. Rev. B **83**, 139901(E) (2011)].
[44] M. Eschrig, A. Cottet, W. Belzig, J. Linder, General boundary conditions for quasiclassical theory of superconductivity in the diffusive limit: application to strongly spin-polarized systems, New J. Phys. **17**, 083037 (2015).
[45] A. Kamra, A. Rezaei, and W. Belzig, Spin Splitting Induced in a Superconductor by an Antiferromagnetic Insulator, Phys. Rev. Lett. **121**, 247702 (2018).
[46] See Supplementary material at
[47] G. S. D. Beach, C. Nistor, C. Knutson, M. Tsoi and J. L. Erskine, Dynamics of field-driven domain-wall propagation in ferromagnetic nanowires, Nat. Mater. **4**, 741 (2005).
[48] G. S. D. Beach, C. Knutson, C. Nistor, M. Tsoi, and J. L. Erskine, Nonlinear Domain-Wall Velocity Enhancement by Spin-Polarized Electric Current, Phys.Rev. Lett. **97**, 057203 (2006).
[49] J. Mendil, M. Trassin, Q. Bu, J. Schaab, M. Baumgartner, C. Murer, P. T.Dao, J. Vijayakumar, D. Bracher, C. Bouillet, C. A. F. Vaz, M. Fiebig, and P. Gambardella, Magnetic properties and domain structure of ultrathin yttrium iron garnet/Pt bilayers, Phys. Rev. Mat. **3**, 034403 (2019).
[50] I. V. Bobkova, Yu. S. Barash, Effects of spin-orbit interaction on superconductor ferromagnet heterostructures: spontaneous electric and spin surface currents, Pisma v Zh. Eksper. Teoret. Fiz. **80**, 563 (2004).
[51] R. Grein, M. Eschrig, G. Metalidis, and Gerd Schon, Spin-Dependent Cooper Pair Phase and Pure Spin Supercurrents in Strongly Polarized Ferromagnets, Phys. Rev. Lett. **102**, 227005 (2009).
[52] M. Alidoust, J. Linder, G. Rashedi, T. Yokoyama, and A. Sudbo, Spin-polarized Josephson current in superconductor/ferromagnet/superconductor junctions with inhomogeneous magnetization, Phys. Rev. B **81**, 014512 (2010).
[53] Z. Shomali, M. Zareyan, W. Belzig, Spin supercurrent in Josephson contacts with noncollinear ferromagnets, New J. Phys. **13**, 083033 (2011).
[54] M. Alidoust, and K. Halterman, Spontaneous edge accumulation of spin currents in finite-size two-dimensional diffusive spinorbit coupled SFS heterostructures, New J. Phys. **17**, 033001 (2015).
[55] K. Halterman, O.T. Valls, and C.-T. Wu, Charge and spin currents in ferromagnetic Josephson junctions, Phys. Rev. B **92**, 174516 (2015).
[56] S. Jacobsen, I. Kulagina, J. Linder, Controlling superconducting spin flow with spin-flip immunity using a single homogeneous ferromagnet, Sci. Rep. **6**, 23926 (2016).
[57] F. Konschelle, I. V. Tokatly, F. S. Bergeret, Ballistic Josephson junctions in the presence of generic spin dependent fields, Phys. Rev. B **94**, 014515 (2016).
[58] F. Aikebaier, P. Virtanen, and T. Heikkila, Superconductivity near a magnetic domain wall, Phys. Rev. B **99**, 104504 (2019).
[59] Z. Li, J. He, and S. Zhang, Effects of spin current on ferromagnets, J. Appl. Phys. **99**, 08Q702 (2006).
[60] M. Eschrig, Distribution functions in nonequilibrium theory of superconductivity and Andreev spectroscopy in unconventional superconductors, Phys. Rev. B **61**, 9061 (2000).
[61] M. Eschrig, Scattering problem in nonequilibrium quasiclassical theory of metals and superconductors: General boundary conditions and applications, Phys. Rev. B **80**, 134511 (2009).
[62] A. Stern, Berrys phase, motive forces, and mesoscopic conductivity, Phys. Rev. Lett. **68**, 1022 (1992).
[63] M. Stone, Magnus force on skyrmions in ferromagnets and quantum Hall systems, Phys. Rev. B **53**, 16573 (1996).
[64] G. E. Volovik, Linear momentum in ferromagnets, J. Phys. C **20**, L83 (1987).
[65] L. Berger, Possible existence of a Josephson effect in ferromagnets, Phys. Rev. B **33**, 1572 (1986).
[66] S.E. Barnes and S. Maekawa, Generalization of Faradays Law to Include Nonconservative Spin Forces, Phys. Rev. Lett. **98**, 246601 (2007).
[67] R. A. Duine, Spin pumping by a field-driven domain wall, Phys. Rev. B **77**, 014409 (2008).

[68] W. M. Saslow, Spin pumping of current in non-uniform conducting magnets, Phys. Rev. B **76**, 184434 (2007).

[69] Y. Tserkovnyak and M. Mecklenburg, Electron transport driven by nonequilibrium magnetic textures, Phys. Rev. B **77**, 134407 (2008).

[70] S. Zhang and S. S.-L. Zhang, Generalization of the Landau-Lifshitz-Gilbert Equation for Conducting Ferromagnets, Phys. Rev. Lett. **102**, 086601 (2009).

[71] S. A. Yang, G. S. D. Beach, C. Knutson, Di Xiao, Q. Niu, M. Tsoi, and J. L. Erskine, Universal Electromotive Force Induced by Domain Wall Motion, Phys. Rev. Lett. **102**, 067201 (2009).

[72] S. A. Yang, G. S. D. Beach, C. Knutson, Di Xiao, Z. Zhang, M. Tsoi, Q. Niu, A. H. MacDonald, and J. L. Erskine, Topological electromotive force from domain-wall dynamics in a ferromagnet, Phys. Rev. B **82**, 054410 (2007).

[73] D.S. Rabinovich, I.V. Bobkova, A.M. Bobkov, and M.A. Silaev, Resistive state of SFS Josephson junctions in the presence of moving domain walls, arXiv:1904.03449

[74] D.S. Rabinovich, I.V. Bobkova, A.M. Bobkov, Electrical response of S-F-TI-S junctions on magnetic texture dynamics, arXiv:1904.11193